Journal of Earthquake and Tsunami
Vol. 11, No. 1 (2017) 1740001 (26 pages)

DOI: 10.1142/S1793431117400012

Implications of Local Sources to Probabilistic Tsunami Hazard Analysis in South Chinese Coastal Area

Yeifei Ren*, Ruizhi Wen and Peng Zhang

Key Laboratory of Earthquake Engineering and Engineering Vibration
Institute of Engineering Mechanics, China Earthquake Administration
Harbin 150080, China
**renyefei@iem.net.cn*

Zhibo Yang and Rong Pan

Nuclear and Radiation Safety Center
Ministry of Environmental Protection of the People's Republic of China
Beijing 100082, China

Xiaojun Li

Institute of Geophysics
China Earthquake Administration
Beijing 100022, China

Received
Accepted 29 September 2016
Published

The South China Sea is recognized as an area at high risk of tsunamis. The Manila Trench has long been considered as the regional source of tsunamis that might affect Chinese coastal areas, and considerable analysis of the tsunami hazard has been conducted in this area. However, there has been no consideration of other potential local sources near the coastal area. Thus, the locations of local potential tsunami sources (PTSs) along the southern coast of China and the evaluation of their impact on tsunami hazard assessment require investigation. We identified eight local PTSs for given seismic activity parameters. For the probabilistic tsunami hazard analysis (PTHA), the lower-limit earthquake magnitude was determined as 7.0, based on numerical simulation of tsunami scenarios. Six measured sites in the Pearl River Estuary and Taiwan Strait were selected for PTHA, which were referenced to Macao, Hong Kong, Daya Bay, Shantou, Xiamen, and Quanzhou. The annual rate of tsunami waves exceeding a given height ($h \geq H$) was calculated for each site. The results show that the upper-limit earthquake magnitude and the relative geographical positions of the measured site of interest and the PTS are two of the most important factors in the PTHA computation. The probabilities of tsunami waves exceeding a given height ($h \geq H$) within 100 years and their return periods were calculated for each site. The results show that the probability of $h \geq 0.5$ m within 100 years is 30–40% in Xiamen and Quanzhou but 5–10% in Macao and Hong Kong. If the Manila Trench were considered as a regional source, these probabilities would be higher. It is concluded that the tsunami hazard on the southern coast

*Corresponding author.

of China is very high and that both regional and local PTSs should be included in any future PTHA.

Keywords: Probabilistic tsunami hazard analysis; potential local tsunami source; zonation map; seismic activity; Monte Carlo technique; numerical simulation; South China Sea.

1. Introduction

In ancient Chinese literature, the word "haiyi" or "chaoyong" is used to describe any abnormal rise and fall of sea level. This makes it difficult to distinguish between tsunami and storm-surge events in historical records, and it can lead to the misapprehension that few tsunamis have affected China in the past [Mak and Chan, 2007; Chau, 2008; Lau *et al.*, 2010; Ren *et al.*, 2014]. Coastal areas of China have not been affected by any destructive tsunamis during the last 100 years and consideration of the tsunami hazard has been neglected. However, the 2004 Sumatra and 2011 Tohoku earthquakes and tsunamis caused considerable numbers of casualties and large economic losses, which raised the awareness of the Chinese government and population to the danger posed by tsunamis.

The Pearl River Delta economic circle in Southeast China, which includes major cities such as Hong Kong, Macau, and Shenzhen, comprises part of the most economically developed area of the country. Coastal areas such as Fuzhou, Quanzhou, and Xiamen are also developed based on economic exchange with Taiwan. The increasingly important major infrastructure projects, such as the Hong Kong-Zhuhai-Macao Bridge, and the Dayawan and Yangjiang nuclear power plants have been built or are planned to be built along the coastline. Therefore, it is imperative that a comprehensive evaluation of the tsunami hazard in this area be undertaken. Assessments of the tsunami hazard in the South China Sea (SCS) have been performed in recent years by both Chinese scientists [Wen and Ren, 2007; Liu *et al.*, 2007; Pan *et al.*, 2009; Ren *et al.*, 2010, 2014; Wen *et al.*, 2011; Hou *et al.*, 2016] and international researchers [Dao *et al.*, 2009; Huang *et al.*, 2009; Liu *et al.*, 2009; Megawati *et al.*, 2009; Wu and Huang 2009; Okal *et al.*, 2011; Suppasri *et al.*, 2012]. However, these studies have focused mostly on the potential tsunami hazard by considering the regional source as the Manila Trench; the influence from any other local source along the Chinese coast has been largely overlooked. Some studies have shown that the seismic tectonics of the Chinese coastal area of the SCS could trigger a destructive tsunami [Zhang, 1995; Yang and Wei, 2005]. Historical records have revealed that some destructive earthquakes have occurred within this area, which then triggered damaging tsunamis [Mak and Chan, 2007; Ren *et al.*, 2014]. For example, an M 7.5 earthquake on December 19, 1604 in Quanzhou (Fujian Province) and an M 7.3 earthquake on February 13, 1918 in Shantou (Guangdong Province) both generated tsunami waves.

Given the socioeconomic importance of Southeast China, the locations of local potential tsunami sources (PTSs) along the southern coast and the evaluation of

their impact on tsunami hazard require investigation. In this study, we identified eight local PTSs for given seismic activity parameters, and with reference to the method of probabilistic seismic hazard analysis, the method of probabilistic tsunami hazard analysis (PTHA) was used for the investigation. The probabilities of tsunami waves exceeding a given height were calculated for some typical sites within the Pearl River Delta and Taiwan Strait regions. The results reported in this paper provide scientific support for further studies of the effects of local sources on probabilistic tsunami hazard analyses of the southern coastal area of China.

2. Potential Tsunami Sources

The Manila Trench is where the Eurasian Plate is subducting beneath the Philippine Plate and it is a region of frequent earthquakes, which have elevated concern regarding the tsunami hazard in the SCS. Consequently, most previous studies have focused on the Manila Trench as the regional PTS, rather than PTSs along the Chinese coast.

In June 2015, the fifth-generation national "Seismic ground motion parameters zonation map of China (GB 18306−2015)" was issued. It takes almost five years to accomplish this map by a big team including many geologists, geophysicists, seismologists, engineers, etc. Totally 1206 potential seismic sources (PSSs) are delineated across the entire country and some neighboring areas (Fig. 1). Supposing

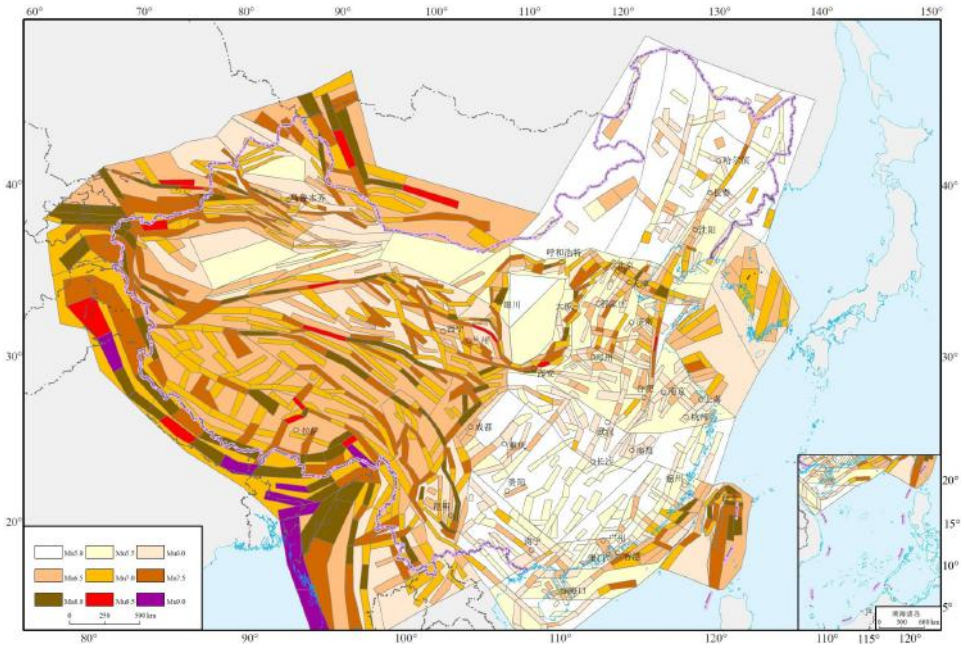

Fig. 1. Potential earthquake sources delineated by the fifth-generation national zonation map of seismic ground motion parameters of China.

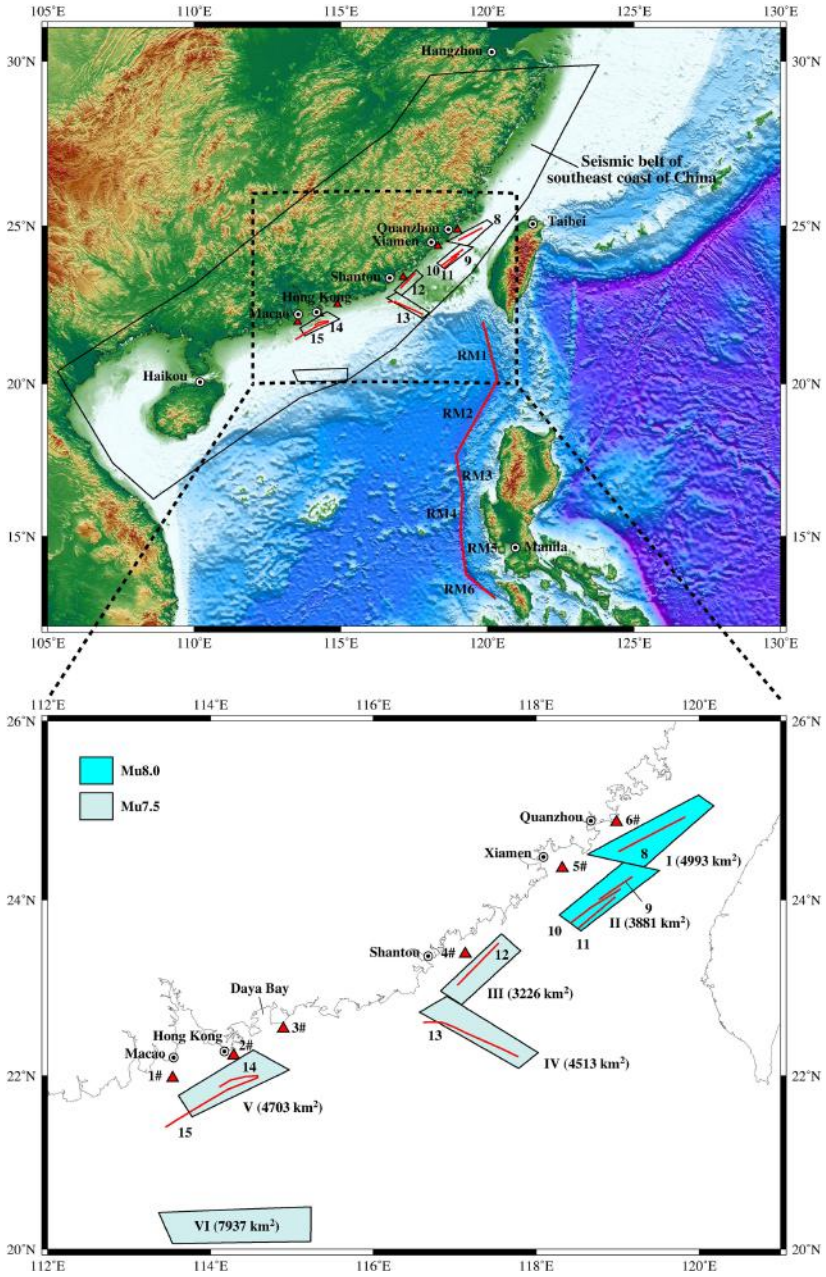

Fig. 2. Local and regional PTSs affecting the Chinese coastal area of the SCS. Regional PTSs RM1–RM6 were derived from Ren *et al.* [2014]. Local PTSs (Nos. 8–15) were determined by Chen and Zhou [2011] and Ren *et al.* [2014]. The polygon defines the seismic belt of the southeast coast of China, which was used for calculating the parameters of seismic activity for each PSS. The six quadrilaterals delineate the PSSs identified by the seismic ground motion parameter zonation map of China. The areas of the PSSs are marked in parentheses. The upper limits of the earthquake magnitudes of the PSSs are indicated by different colors. Numbers 1# to 6# mean the locations where the PTHA was performed for the case studies in the following text.

Table 1. Locations and earthquake source parameters of the eight local PTSs affecting the Chinese coastal area of the SCS.

No.	Name	Node location		Strike (°)	Length (km)	Width (km)	Average depth (km)	Dip (°)	Rake (°)	Upper-limit magnitude (M_u)
		Node	Longtitude (°E)	Latitude (°E)						
8	Quanzhou	Q1	119.01	24.54	65	92	71	20	60	90	8.0
		Q2	119.83	24.93							
9	Xiamen No. 1	XM1	118.77	24.00	58	51	71	20	60	90	8.0
		XM2	119.18	24.26							
10	Xiamen No. 2	XM3	118.43	23.74	57	74	71	20	60	90	8.0
		XM4	118.67	23.91							
		XM5	119.04	24.12							
11	Xiamen No. 3	XM6	118.52	23.68	53	59	71	20	60	90	8.0
		XM7	118.97	24.03							
12	Nan'ao	BN1	117.03	23.03	47	75	50	20	60	90	8.0
		BN2	117.54	23.51							
13	Taiwan	TW1	116.61	22.61	118	130	50	20	60	90	7.5
		TW2	116.84	22.61							
		TW3	116.98	22.56							
		TW4	117.18	22.47							
		TW5	117.55	22.32							
		TW6	117.77	22.22							
		TW7	117.78	22.22							
14	Zhu-Ao	ZA1	114.11	21.87	74	52	50	20	60	90	7.5
		ZA2	114.25	21.95							
		ZA3	114.43	21.99							
		ZA4	114.59	22.00							
15	Dan'gan	DG1	113.45	21.41	63	135	50	20	60	90	7.5
		DG2	113.83	21.63							
		DG3	114.21	21.84							
		DG4	114.59	21.98							

same locations with PTSs, some of these PSSs were used to determine the local PTSs by Chen and Zhou [2011] and Ren *et al.* [2014] depending on their upper-limit earthquake magnitude, seismic tectonic setting, seismic activity, and other parameters. Consequently 15 local PTSs were delineated, and 8 of them in the SCS (Nos. 8–15; Fig. 2) were selected for consideration in this study. It should be noted that only those PSSs located within the Taiwan Strait were selected for this study, rather than those located to the east of Taiwan. This was because it is believed that Taiwan protects the Chinese mainland from the effects of tsunamis generated to the east. Figure 2 also shows the six regional PTSs (Nos. RM1–RM6) in the Manila Trench, as given by Ren *et al.* [2014]. Because this study considered only the roles of local PTSs, the importance of the combination of both local and regional PTSs to the PTHA will be discussed in further study.

Table 1 presents the geographical locations and earthquake source parameters of the eight PTSs used for the PTHA. Except the rake angle, other parameters were estimated by Chen and Zhou [2011] according to a comprehensive analysis on the investigation on tectonic stress, statistics of historical earthquakes, observation of geophysical field, and even personal experiences of some seismologist, etc. For estimating the rake angle, they assumed all PTSs as thrust-type faults that means rake angle equals to 90° for each PTS. Some evidences show a possibility of strike-slip stress mechanism for some PTSs, such as PTS No. 8 where the 1604 M8.0 Quanzhou earthquake occurred in. The focal mechanism and stress analysis of this earthquake represent strike-slip mechanism is favorable in this region [Zhou and Chen, 1983; Zheng *et al.*, 2011]. However, so far there is not any powerful proof provided by modern instrumental survey or geophysical knowledge to predict an exact rage angle for the scenario earthquake occurred any fault along the Chinese coast. For the sake of safety, the worst case supposing all the faults as thrust type is proposed in the study of Chen and Zhou [2011]. Such kind of proposal is also used in the study of Wu [2012] which evaluated the potential tsunami hazard in Taiwan by a deterministic analysis.

For the PTHA, it is necessary to know the other parameters, such as the upper limit of the earthquake magnitude M_u, constant b in the Gutenberg−Richter law, and the annual rate of occurrence of an earthquake v, which will be discussed in the following text.

3. Numerical Simulation of Tsunami Scenarios

Before conducting the PTHA for the local sources, we performed numerical simulations of the propagation processes of two tsunami scenarios to analyze the characteristics of each local source. The two scenarios involved modeling earthquake magnitudes of M_{w}7.0 and M_{w}7.5 at PTS sites Nos. 13–15. The value of M_{w}7.5 is the upper-limit earthquake magnitude of these PTSs (see Table 1).

The ruptured length and width of the fault were determined from empirical relationships given by Wells and Coppersmith [1994], which are scaled according to the

magnitude. Wells and Coppersmith [1994] also developed an empirical relationship between the magnitude and average slip, but this correlation coefficient is only 0.1 (see Table 2B of Wells and Coppersmith [1994]). Therefore, the average slip in this study was estimated using the following equation [Aki, 1966]:

$$M_0 = \mu LWD, \tag{1}$$

where M_0 is the scalar moment of the earthquake, coefficient μ is the shear rigidity of the Earth's crust, L and W represent the length and width of the fault plane, respectively, and D is the amount of average slip. Parameter μ is related to the density ρ and shear velocity V_S of the Earth's crust:

$$V_S = \sqrt{\frac{\mu}{\rho}}. \tag{2}$$

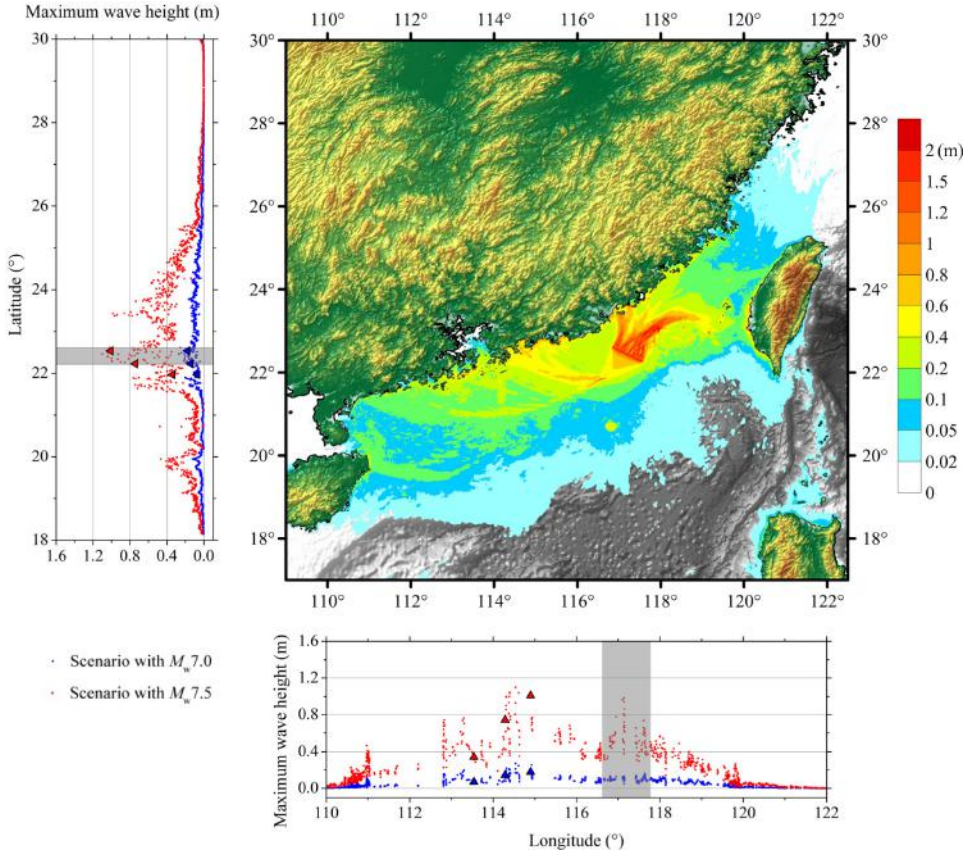

Fig. 3. Tsunami wave heights along the Chinese coast when M_w7.0 and M_w7.5 scenario earthquakes occur at PTS No. 13. The middle figure presents the distribution of maximum wave height for the M_w7.5 scenario. Shaded areas indicate the projection of PTS No. 13 at the corresponding longitude and latitude. Red and blue triangles show the wave heights at the three sites of interest for which the PTHA was conducted.

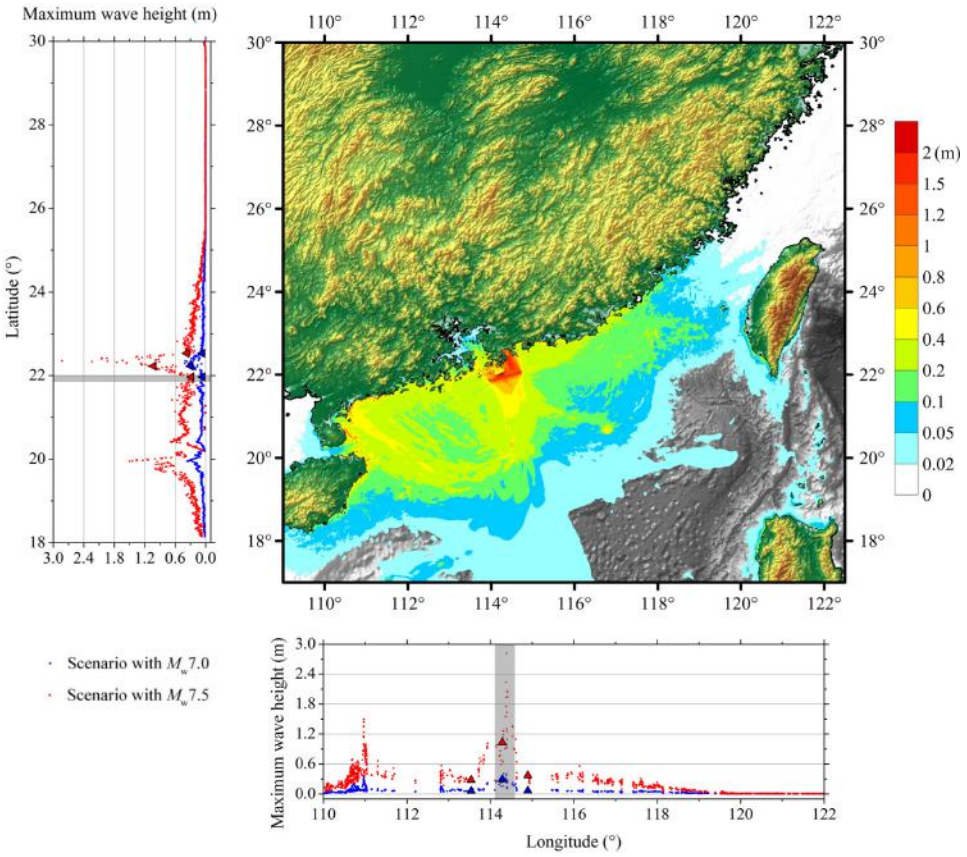

Fig. 4. Tsunami wave heights along the Chinese coast when M_w7.0 and M_w7.5 scenario earthquakes occur at PTS No. 14. The middle figure presents the distribution of maximum wave height for the M_w7.5 scenario.

Usually the mean values of ρ and V_S of the shallow crust are estimated as 2.7 g/cm^3 and 3.6 km/s, respectively, for the Chinese mainland [Pei *et al.*, 2004]. Consequently, μ is equal to 35 Gpa based on the above formulas.

The value of M_0 can be determined using the following equation [Hanks and Kanamori, 1979]:

$$M_w = \frac{2}{3}\log M_0 - 10.7, \tag{3}$$

where M_w is the moment magnitude of an earthquake; here, given as 7.0 and 7.5.

The open-source Cornell Multi-grid Coupled Tsunami Model is commonly used for simulations. Here, the linear shallow-water wave equation was employed rather than the nonlinear model. The linear treatment can serve our purposes sufficiently, as has been verified already by Liu *et al.* [2007]. A run-up stage was not included in this study. More than 1200 measured sites were selected from the 10-m isobath

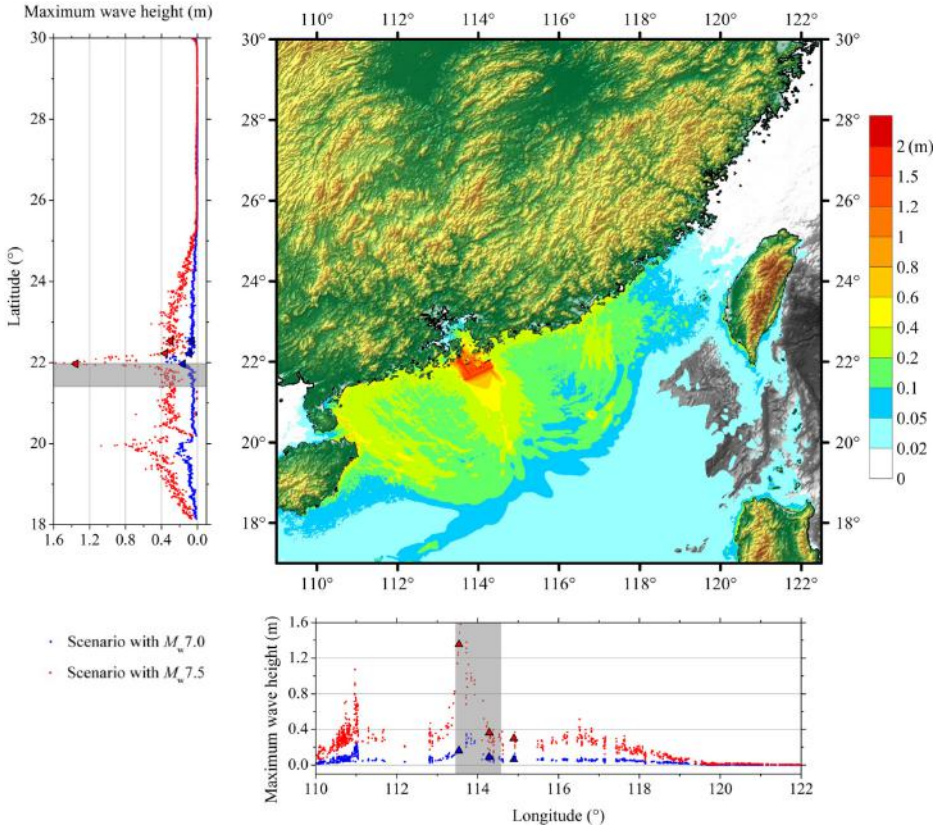

Fig. 5. Tsunami wave heights along the Chinese coast when M_w7.0 and M_w7.5 scenario earthquakes occur at PTS No. 15. The middle figure presents the distribution of maximum wave height for the M_w7.5 scenario.

along the Chinese coast. Figures 3–5 show the distribution of simulated wave height associated with each tsunami scenario for PTS Nos. 13–15, respectively.

The maximum wave height at the measured sites is estimated to be about 1.2 m for an M_w7.5 earthquake at PTS No. 13 (Fig. 3), 3 m for an earthquake at PTS No. 14 (Fig. 4), and 1.6 m for an earthquake at PTS No. 15 (Fig. 5). Although the wave height is lower, PTS No. 13 affects a much wider region than the other two PTSs, not only in the Pearl River Estuary (where sites 1#, 2#, and 3# are located; see Fig. 2) but also in the Taiwan Strait (where sites 4#, 5#, and 6# are located; see Fig. 2). For tsunamis generated at PTS Nos. 14 and 15, the large wave heights only appear in those regions perpendicular to the faults (see Figs. 4 and 5). The reasonable explanation for this is that the fault strike for PTS Nos. 14 and 15 is parallel to the coastline, whereas it is oblique to the coastline for PTS No. 13. Thus, PTS Nos. 14 and 15 were selected for the PTHA as case studies for sites 1#, 2#, and 3#, PTS Nos. 8–12 were considered for sites 4#, 5#, and 6#, and PTS No. 13 was considered for all of the sites.

Figures 3–5 show that for an M_w7.0 earthquake occurring at PTS Nos. 13–15, the resulting tsunami wave heights at all sites are very small, i.e. mostly <0.2 m. Therefore, the lower-limit earthquake magnitude for each PTS is suggested to be 7.0 in the following PTHA.

4. PTHA Method

The concept and computational procedure of PTHA generally follows the method of probabilistic seismic hazard analysis developed originally by Cornell [1968]. Houston *et al.* [1977] evaluated the tsunami hazard for the Hawaiian Islands using this method, and it has been used subsequently in other countries, including Japan [Rikitake and Aida, 1988], Italy [Tinti, 1991], New Zealand [Kelvin, 2005], and Peru [Kulikov *et al.*, 2005]. The principles and method of PTHA have been systemically rearranged and proposed by Geist and Parsons [2006] for the evaluation of the tsunami hazards in Acapulco (Mexico) and Cascadia (USA) using both historical data and numerical simulation results. The logic-tree approach was applied to PTHA by Annaka *et al.* [2007] and an improved PTHA method using Bayesian theory was proposed by Grezio *et al.* [2010]. Subsequently, PTHA has been adopted for many other studies in various locations, such as Thailand [Suppasri *et al.*, 2012], Western Australia [Burbidge *et al.*, 2008], Southeast China [Liu *et al.*, 2007], Southeast Asia [Thio *et al.*, 2007], Oregon (USA) [González *et al.*, 2009], California (USA) [Thio *et al.*, 2010], and the Mediterranean Sea [Papadopoulos *et al.*, 2010].

The procedure of probabilistic seismic hazard analysis has been used in China for the compilation of the zonation map of seismic ground motion parameters [Gao, 2015]. With reference to this procedure, we proposed the following method for PTHA in China.

For an earthquake occurring within a region, the cumulative distribution function (CDF) $F(M)$ and probability density function (PDF) $f(M)$ of its magnitude M can be expressed as:

$$F(M) = \frac{1 - \exp[-\beta(M - M_{\min})]}{1 - \exp[-\beta(M_{\max} - M_{\min})]}, \quad M_{\min} \le M \le M_{\max}, \tag{4}$$

$$f(M) = \frac{\beta \exp[-\beta(M - M_{\min})]}{1 - \exp[-\beta(M_{\max} - M_{min})]}, \quad M_{\min} \le M \le M_{\max}, \tag{5}$$

where $M_{\max}$ and $M_{\min}$ are the possible maximum and minimum magnitudes for an earthquake occurring within this region, $\beta = b \cdot \ln 10$, and b is a statistical constant of the Gutenberg−Richter recurrence law.

Suppose N_i earthquakes happen at the ith PTS. Their spatial locations and magnitudes can be produced randomly using the Monte Carlo technique. The N_i magnitudes should meet the PDF (Eq. (5)) of this PTS. The value of $M^i_{\max}$ should be the upper-limit earthquake magnitude M_{ui} of this PTS, i.e. 7.5 or 8.0 in this study (see Fig. 2), and the value of $M^i_{\min}$ (7.0) is the lower-limit earthquake

magnitude proposed previously. Here, we use M_1^i and M_2^i instead of $M_{\min}^i$ and $M_{\max}^i$, respectively.

For the site of interest, N_i values of maximum wave height can be obtained by numerical simulation of the tsunami generation and propagation processes trigged by these N_i earthquakes. The length, width, and average slip of the fault plane for each earthquake occurring within the local PTSs were determined as discussed above. For an earthquake occurring in a regional PTS, e.g. the Manila Trench, it is suggested that these parameters be determined by empirical relationships given by Papazachos *et al.* [2004], which are suitable for a subduction earthquake.

Based on the statistics of historical data, Choi *et al.* [2002, 2012] found that tsunami wave heights follow a lognormal distribution. The PDF of tsunami wave height can be expressed as

$$f_i(h) = \frac{1}{\sqrt{2\pi}h\sigma} \exp\left(-\frac{[\ln(h) - \mu]^2}{2\sigma^2}\right), \tag{6}$$

where h is wave height, and μ and σ are the mean value and standard deviation of $\ln(h)$, respectively, which can be calculated using the N_i values of maximum wave height. Then, we can compute the CDF of the tsunami wave exceeding a given height H by taking the integral of the PDF:

$$F_i(h \geq H) = \int_H^\infty f_i(h)dh = \frac{1}{\sqrt{2\pi}\sigma} \int_H^\infty \exp\left(-\frac{[\ln(h) - \mu]^2}{2\sigma^2}\right) \frac{dh}{h}. \tag{7}$$

If the annual rate of occurrence of earthquakes greater than M_1^i and less than M_2^i at the ith PTS, i.e. $v_i(M_1^i \leq M \leq M_2^i)$, is known, the annual rate of occurrence of tsunami waves from the ith PTS that exceed a given height H, i.e. $v_i(h \geq H)$, can be calculated as

$$v_i(h \geq H) = F_i(h \geq H) \cdot v_i(M_1^i \leq M \leq M_2^i). \tag{8}$$

The procedure to compute $v_i(M_1^i \leq M \leq M_2^i)$ is presented in the following text.

For sites of interest affected by multiple PTSs, the contributions from each PTS should be considered in combination:

$$v(h \geq H) = 1 - \prod_{i=1}^{N_T} [1 - v_i(h \geq H)], \tag{9}$$

where N_T is the total number of PTSs and $v(h \geq H)$ is the total result of the annual rate of $h \geq H$.

Therefore, the return period is

$$R(h \geq H) = \frac{1}{v(h \geq H)}. \tag{10}$$

Under the assumption of the Poissonian occurrence of earthquakes, the probability of observing at least one event $h \geq H$ within period T is equal to

$$P(h \geq H, t = T) = 1 - \exp(-v(h \geq H) \cdot T). \tag{11}$$

5. Seismic Activity Parameters for PTHA

For PTHA, three input parameters must be known for each PTS: b_i, M_{ui}, and $v_i(M_1^i \leq M \leq M_2^i)$. These three parameters characterize the seismic activity within the region of each individual PTS and therefore, their values for a specific PTS are identical to those of the collocated PSS. Figure 2 shows that the locations of the eight PTSs match the six PSSs expressed by the six quadrilaterals and marked by the Roman numerals. The areas of the delineated regions of each individual PSS are also presented in Fig. 2.

The upper-limit earthquake magnitudes for all 1206 PSSs are given in the Chinese national zonation map (Fig. 1) and Table 2 lists those for the six PSSs used in this study. Usually, the region of a single PSS is too small to collect adequate data on historical earthquake events for the analysis of seismicity; therefore, 29 seismic belts are delineated across China within this zonation map. Each seismic belt includes dozens of PSSs but with the same values of b_{belt} (value of b of the Gutenberg−Richter recurrence law within this belt) and v_{belt} (annual rate of occurrence of earthquakes $M \geq 4.0$ within this belt). The six PSSs used in this study are all located within the seismic belt along the southeast coast of China (see Fig. 2), for which the values of $b_{\text{belt}} = 0.87$ and $v_{\text{belt}} = 5.6$ have been assigned [Gao, 2015].

The b_i value of each PSS was set to b_{belt} (0.87). The annual rate of occurrence of earthquakes associated with different levels of magnitude $v_i(M_j)$ can be calculated using the following equation [Gao, 2015]:

$$v_i(M_j) = v_{\text{belt}}(M_j) \cdot \gamma_i(M_j), \tag{12}$$

where M_j means the jth level of discrete magnitudes ordered by $M_0+(j-1)\cdot\Delta M \leq M_j \leq M_0 + j \cdot \Delta M$, $M_0 = 4.0$ (lower-limit earthquake magnitude for the seismic belt or each PSS), j equals an integer (here, expressed by Roman numerals), $1 \leq j \leq (M_{ui}-M_0)/\Delta M$, ΔM is the discrete interval given as 0.5 for small earthquakes and 0.3 or 0.2 for moderate and large earthquakes in the national zonation map, and $\gamma_i(M_j)$ is the weighting of the ith PSS covering its attributed seismic belt, following the principle:

$$\sum_{i=1}^{N_{Sj}} \gamma_i(M_j) = 1, \tag{13}$$

where N_{Sj} means the number of PSSs at which earthquakes greater than M_j can occur. Determining the value of $\gamma_i(M_j)$ is complex, requiring eight factors that are both subjective and objective [Gao, 2015]. The seismic source area is one of the most important factors and therefore, we consider only this factor in the calculation of $\gamma_i(M_j)$ using the following equation:

$$\gamma_i(M_j) = \frac{A_i(M_j)}{\sum_{i=1}^{N_{Sj}} A_i(M_j)}, \tag{14}$$

where $A_i(M_j)$ means the area of the ith PSS.

Table 2. Parameters of seismic activity for each local PTS used in this study.

No. of PSS	No. of PTS	Name of PTS	b_i	M_{ui}	$A_i(M_j)$ (km^2)	$\gamma_i(M_{VII})$	$\gamma_i(M_{VIII})$	$v_i(M_1^i \leq M \leq M_2^i)$ $\times 10^{-3}$		
								$v_i(M_{VII})$	$v_i(M_{VIII})$	Total
I	8	Quanzhou	0.87	8.0	4993	0.171	0.563	1.485	1.798	3.283
II	9	Xiamen No. 1	0.87	8.0	3881	0.133	0.437	1.154	1.398	2.552
	10	Xiamen No. 2								
	11	Xiamen No. 3								
III	12	Nan'ao	0.87	7.5	3226	0.110	0.000	0.959	0.000	0.959
IV	13	Taiwan	0.87	7.5	4513	0.154	0.000	1.342	0.000	1.342
V	14	Zhu-Ao	0.87	7.5	4703	0.161	0.000	1.399	0.000	1.399
	15	Dan'gan								
VI				7.5	7937	0.271	0.000	2.361	0.000	2.361
Total					29,253	1	1	8.700	3.196	11.896

In this study, $\Delta M = 0.5$ was set equal to the interval value of M_{ui} (see Fig. 1). Because M_1^i is determined as 7.0 and M_2^i is 7.5 or 8.0, there are only two levels for M_j within the range of M_1^i to M_2^i. Therefore, there are two levels (M_{VII} and M_{VIII}) for PSS Nos. I and II because of the upper-limit earthquake magnitude of 8.0 (see Fig. 2), and only one level (M_{VII}) for the other four PSSs ($M_u = 7.5$). The values of $\gamma_i(M_{VII})$ and $\gamma_i(M_{VIII})$ for the six PSSs in this study can be calculated using Eq. (14), as shown in Table 2.

For calculating $v_i(M_1^i \le M \le M_2^i)$, it is necessary to know the value of $v_{\text{belt}}(M_j)$ in Eq. (12), i.e. $v_{\text{belt}}(M_{VII})$ and $v_{\text{belt}}(M_{VIII})$. From Eq. (4), the probabilities of occurrence of magnitudes of M_{VII} and M_{VIII} are calculated as:

$$F_{\text{belt}}(M_{VII}) = F_{\text{belt}}(M = 7.5) - F_{\text{belt}}(M = 7.0), \tag{15}$$

$$F_{\text{belt}}(M_{VIII}) = F_{\text{belt}}(M = 8.0) - F_{\text{belt}}(M = 7.5), \tag{16}$$

where $\beta_{\text{belt}} = b_{\text{belt}} \times \ln 10 = 2.003, M_{\max} = M_u = 7.5$ or 8.0, and $M_{\min} = 4.0$. As a result, $F_{\text{belt}}(M_{VII}) = 1.554 \times 10^{-3}$ and $F_{\text{belt}}(M_{VIII}) = 5.706 \times 10^{-4}$. Then, $v_{\text{belt}}(M_{VII})$ can be calculated by

$$v_{\text{belt}}(M_{VII}) = F_{\text{belt}}(M_{VII}) \cdot v_{\text{belt}}(M \ge 4.0). \tag{17}$$

As a result, $v_{\text{belt}}(M_{VII}) = 8.7 \times 10^{-3}$. In the same way, $v_{\text{belt}}(M_{VIII}) = 3.196 \times 10^{-3}$.

From Eq. (12), $v_i(M_{VII})$ and $v_i(M_{VIII})$ can be calculated, as shown in Table 2.

Finally, the value of $v_i(M_1^i \le M \le M_2^i)$ can be calculated using the following equation:

$$v_i(M_1^i \le M \le M_2^i) = \begin{cases} v_i(M_{VII}), & M_{ui} = 7.5; \\ v_i(M_{VII}) + v_i(M_{VIII}), & M_{ui} = 8.0. \end{cases} \tag{18}$$

All of the results of $v_i(M_1^i \le M \le M_2^i)$ for each PSS are given in Table 2. Noting that since only one factor, the area of PSS is used in this study rather than all eight factors to determine the weighting function $\gamma_i(M_j)$, the caculated $v_i(M_{VIII})$ is therefore lager than $v_i(M_{VII})$ for PSSs No. both I and II. It dose not make sense based on the assumption of the Gutenberg–Richter recurrence law. If some other factors can be used for determining $\gamma_i(M_j)$, the values of $v_i(M_{VIII})$ and $v_i(M_{VII})$ can be adjusted to make sure $v_i(M_{VIII})$ is smaller than $v_i(M_{VII})$. However, we believe the values of $v_i(M_1^i \le M \le M_2^i)$ for each PSS will not be affected too much. A more comprehensive analysis on determination of these parameters will be conducted in further studies.

6. Case Studies of the PTHA

Six typical measured sites were selected from more than 1200 ones mentioned in previous numerical simulation of tsunami scenarios. Three were located in the coastal area of the Pearl River Estuary and the others were in the Taiwan Strait.

6.1. *Pearl river estuary*

The three measured sites selected in the Pearl River Estuary at a bathymetric depth of 10 m are numbered 1#, 2#, and 3#. We randomly produced 50 scenario earthquakes for PTS Nos. 13–15 using the Monte Carlo technique. The epicenters were spaced randomly along the entire length of the fault. The magnitudes followed the theoretical PDFs (Eq. (4)) of the individual PTSs.

Figure 6 shows the spatial distribution of the epicenters and CDF of the magnitudes associated with the 50 scenario earthquakes for PTS No. 15. It can be seen that the epicenters are distributed almost uniformly along the fault and that the magnitude distribution is almost consistent with the theoretical CDF curve. This indicates that the processes of Monte Carlo sampling for both epicenter and magnitude are reasonable, and the results are acceptable for PTS No. 15. It may infer that the results for other PTSs are also probably acceptable. Generally speaking, with a greater number of scenarios, higher accuracy could be achieved; however, because of the limited capacity for the computation, only 50 simulations were conducted.

The processes of tsunami generation and propagation were simulated numerically for 50 scenario earthquakes for each PTS. Some parameters of fault geometry for each scenario earthquake, including the rupture length, width, and average slip, are estimated by some empirical relationships as same as the process described in Sec. 3. Same values are given for earthquakes with same magnitudes. Some other parameters, including the strike, dip and rake angles and focal depth are determined by the values given in Table 1. It implies that the earthquakes occurred in the same PTS have the same values of these parameters. As we know, earthquake is stochastic, that means each above-mentioned parameter may be possibly different

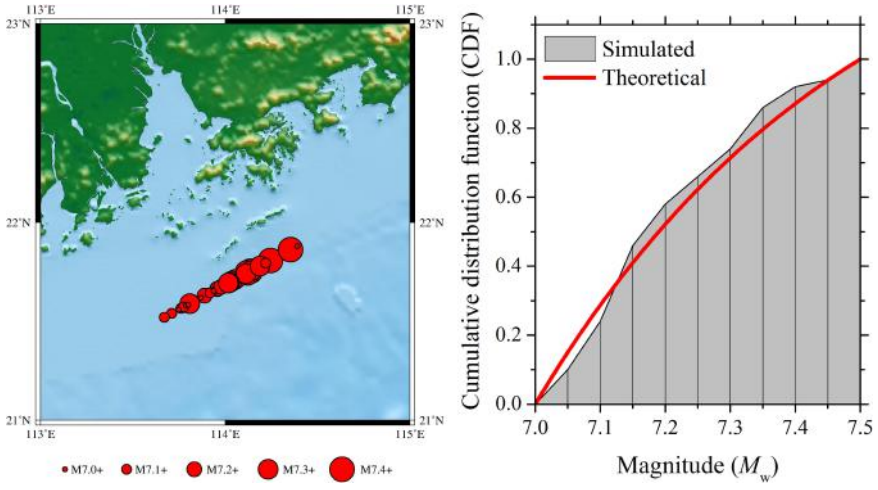

Fig. 6. Locations of 50 earthquakes produced randomly using the Monte Carlo technique for PTS No. 15 (Left panel) and CDF of the magnitudes of these earthquakes (Right panel).

for each earthquake, even occurred in a same fault with a same magnitude. Actually how to accurately predict these parameters is extremely difficult. Therefore, one have to use empirical relationships to determine the fault length, width, and average slip scaling to the size of earthquake magnitude. The strike, dip angles can be determined as fixed values for each PTS by geologists according to the fault tectonics (i.e. Chen and Zhou [2011]), as shown in Table 1. The focal depth is of great importance, assumed to be an average value of 20 km (see Table 1) for each scenario earthquake. Therefore, the uncertainty analysis on the estimation of these parameters should be included in the PTHA computation, which will be conducted in the future work.

Using Eq. (6), the PDFs of the wave height at each site were regressed for the 50 simulations for each PTS, as shown in Fig. 7. The regressed μ and σ are also shown in Fig. 7. The acceptable goodness of fit confirms the assumption that tsunami wave heights follow a lognormal distribution.

Using Eq. (8), the annual rates of occurrence of tsunami waves from PTS Nos. 13–15 exceeding a given height H were calculated for sites 1#, 2#, and 3#, respectively, and the total rate of the combined contributions from the three PTSs were calculated using Eq. (9), as shown in Fig. 8.

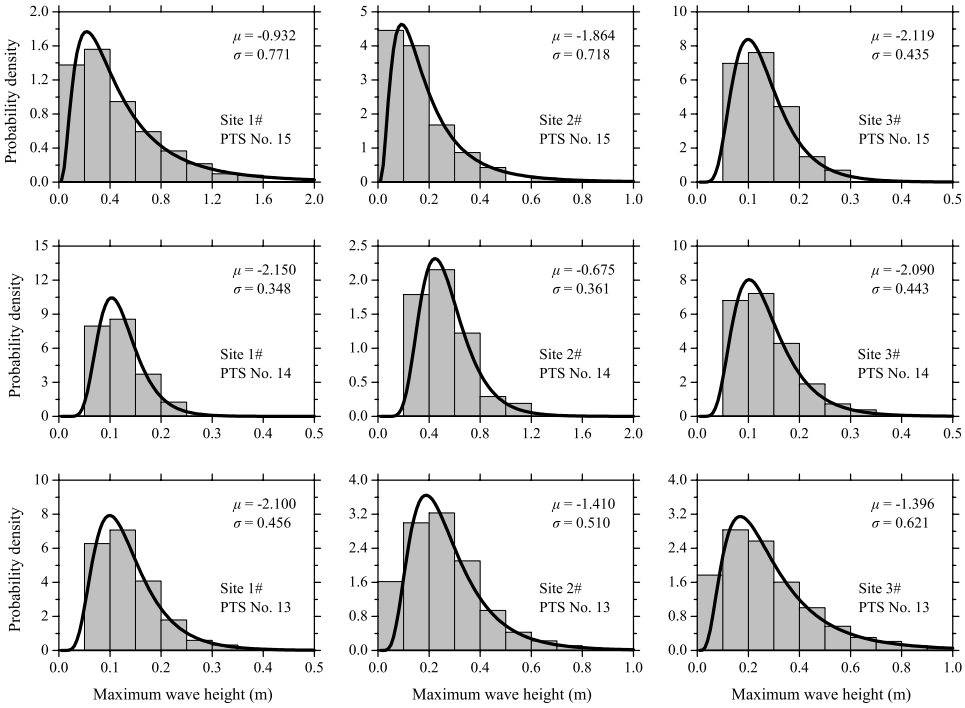

Fig. 7. Regressed PDFs of the 50 maximum tsunami wave heights for sites 1#, 2#, and 3# induced by the 50 scenario earthquakes at PTS Nos. 13–15. Thick curves represent the regressed PDFs. Gray bars represent discrete PDFs calculated using the regressed μ and σ.

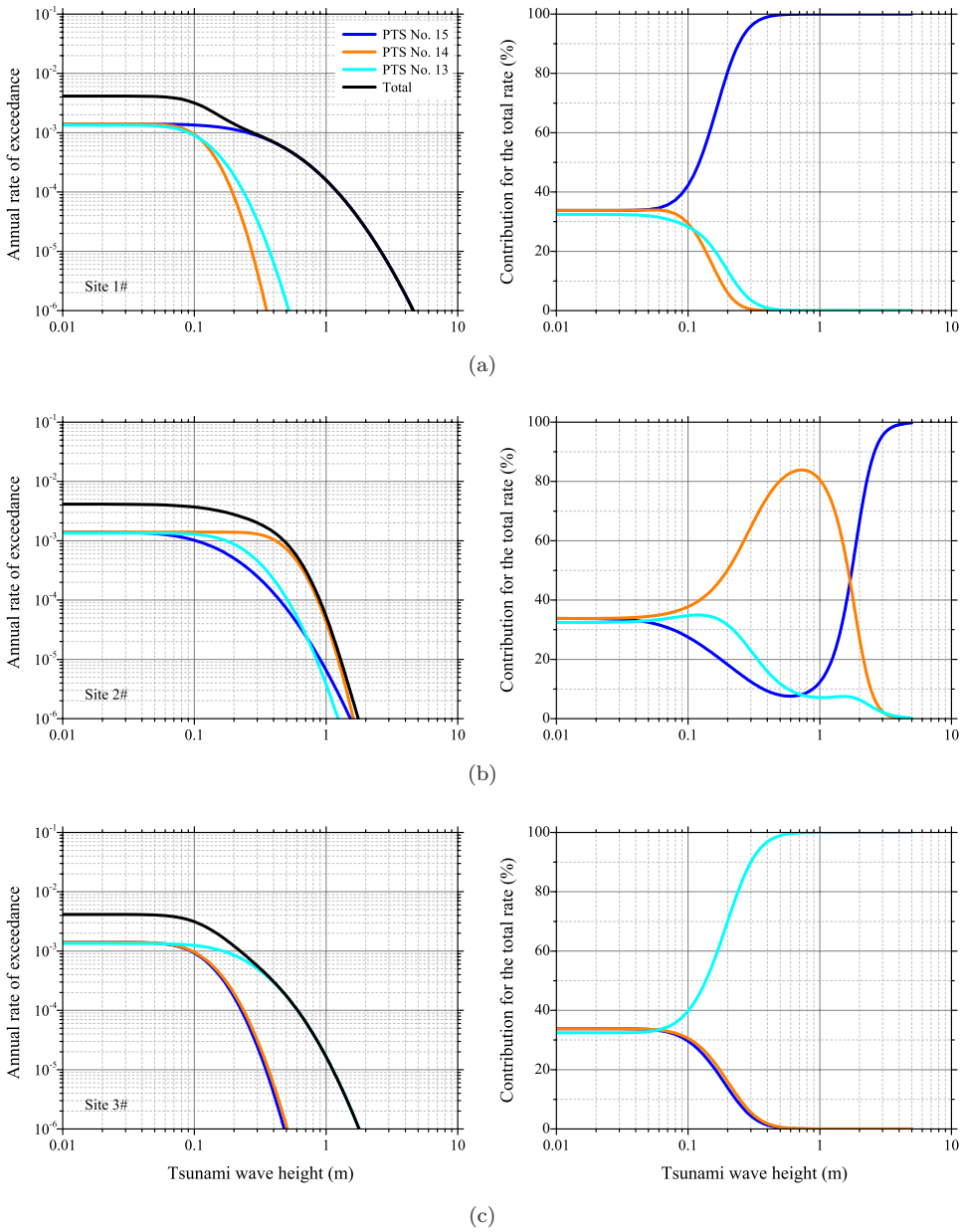

(a)

(b)

(c)

Fig. 8. Annual rate of occurrence of tsunami waves exceeding a given height at sites 1#, 2#, and 3# (Left panels) and contribution of each PTS to the computation of the total rate (Right panels).

The contribution rate of each PTS $\psi_i(h \geq H)$ can be calculated using the following equation:

$$\psi_i(h \geq H) = \frac{v_i(h \geq H) \sum_{J=0}^{N_T-1} \left\{ \sum_{l=1}^{C(N_T-1,J)} \frac{1}{J+1} \prod_{j=1}^{J} v_{j,l} \prod_{k=1}^{N_T-J-1} (1 - v_{k,l}) \right\}}{v_{\text{total}}(h \geq H)}, \tag{19}$$

where $v_{\text{total}}(h \geq H)$ and $v_i(h \geq H)$ mean the total rate and individual rate attributed to ith PTS of tsunami waves exceeding a given height H at the site of interest. $C(N_T - 1, J)$ indicates the maximum number of times, when taking J samples from $(N_T - 1)$ PTSs, for which the ith PTS is not included. The result of each sampling is different and $J = 0, 1, 2, \ldots, N_T - 1$. The parameter $v_{j,l}$ means the annual rate of the jth PTS of J PTSs when taking the lth time of the sampling. The parameter $v_{k,l}$ means the annual rate of the other PTS, except for the ith and jth PTSs. Parameter N_T is the total number of PTSs. As shown in Fig. 8, any value of $v_i(h \geq H) \ll 1$ and therefore, $\psi_i(h \geq H)$ can be approximately equal to the value calculated for $J = 0$ or 1.

Figure 8 shows the total rate of occurrence at sites 1#, 2#, and 3# is predominantly attributed to PTS No. 15, No. 14, and No. 13, respectively. It is dependent on the relative geographical position between the measured site of interest and the PTS (see Fig. 2). It is noted that for the annual rate of occurrence at site 2#, when wave height is >1.0 m, the contribution from PTS No. 14 is decreased, while that from PTS No. 15 is increased. In fact, the wave height at site 2# is <1.0 m if the tsunami is generated at PTS No. 15 (see Fig. 7). The PDFs of wave height >1.0 m were estimated by extrapolation of the data <1.0 m. Future work will confirm whether this is correct; it might be better to have a truncation at a wave height of 1.0 m.

The annual rate of occurrence of tsunami waves exceeding 0.5 m is 5×10^{-4} at site 1#, 8×10^{-4} at site 2#, and 1.5×10^{-4} at site 3#. Site 2# is located between PTS Nos. 13 and 15 (see Fig. 2); thus, it could be affected by tsunamis generated from either. This is why site 2# has the highest risk. Furthermore, PTS No. 13 is aligned obliquely to the coastline, while PTS Nos. 14 and 15 are aligned parallel to the coastline; therefore, the risk at site 3# is lower than at the other two sites. A similar phenomenon can be observed when the wave height is >1.0 m (see Fig. 8).

6.2. *Taiwan strait*

The selected sites 4#, 5#, and 6# are located in the Taiwan Strait, as shown in Fig. 2. As PTS Nos. 14 and 15 have only a minor impact on these three sites (see Figs. 4 and 5), PTS Nos. 8–13 were used for the PTHA. The procedures to determine the epicenter locations and magnitude sizes of scenario earthquakes and to estimate their source parameters are same with those operated in the Pearl River Estuary. The PDFs of simulated tsunami wave height at each site attributed to the individual PTSs are shown in Fig. 9.

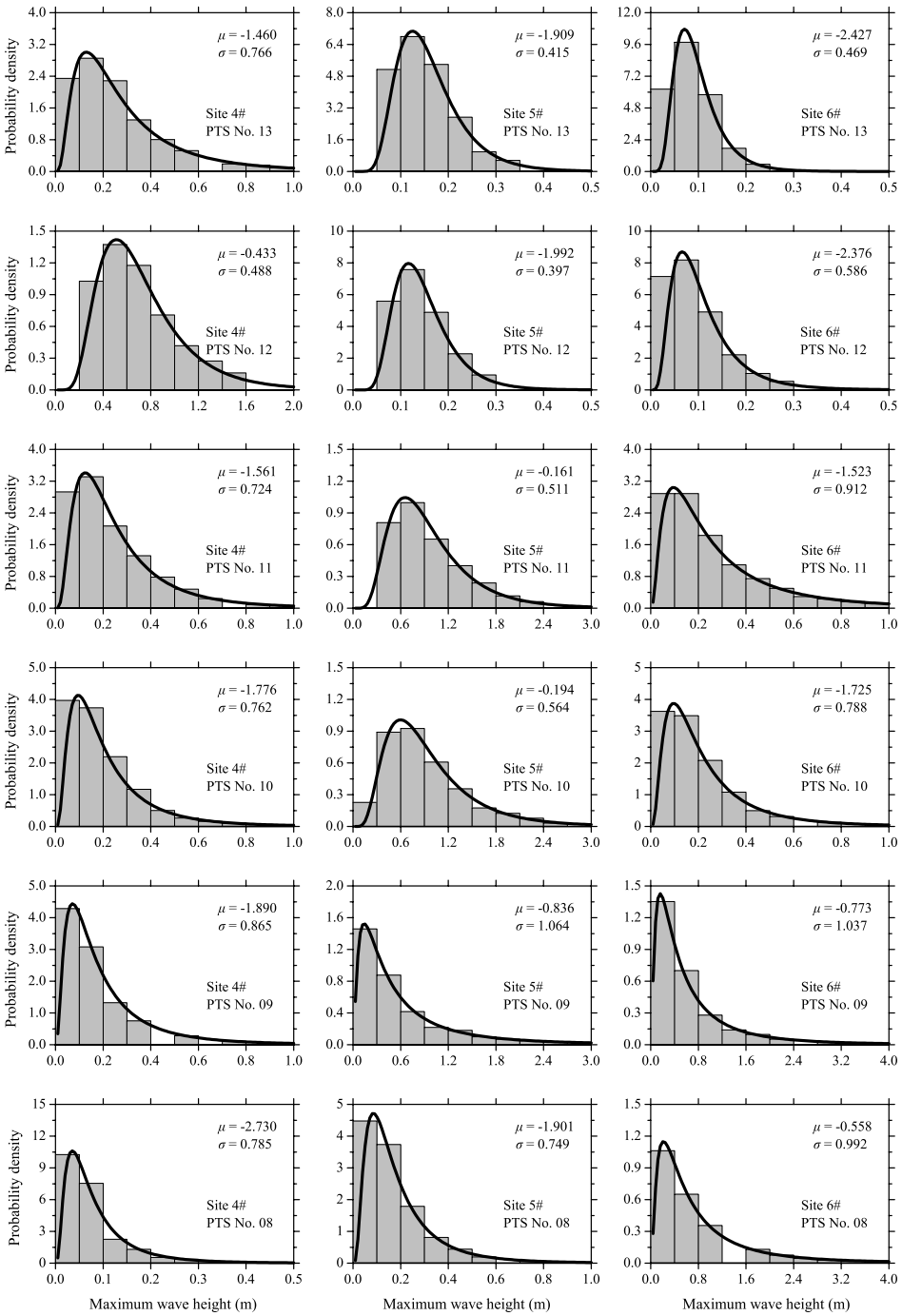

Fig. 9. Regressed PDFs of the 50 maximum tsunami wave heights for sites 4#, 5#, and 6# induced by the 50 scenario earthquakes at PTS Nos. 8–13. Thick curves represent the regressed PDFs. Gray bars represent discrete PDFs calculated using the regressed μ and σ.

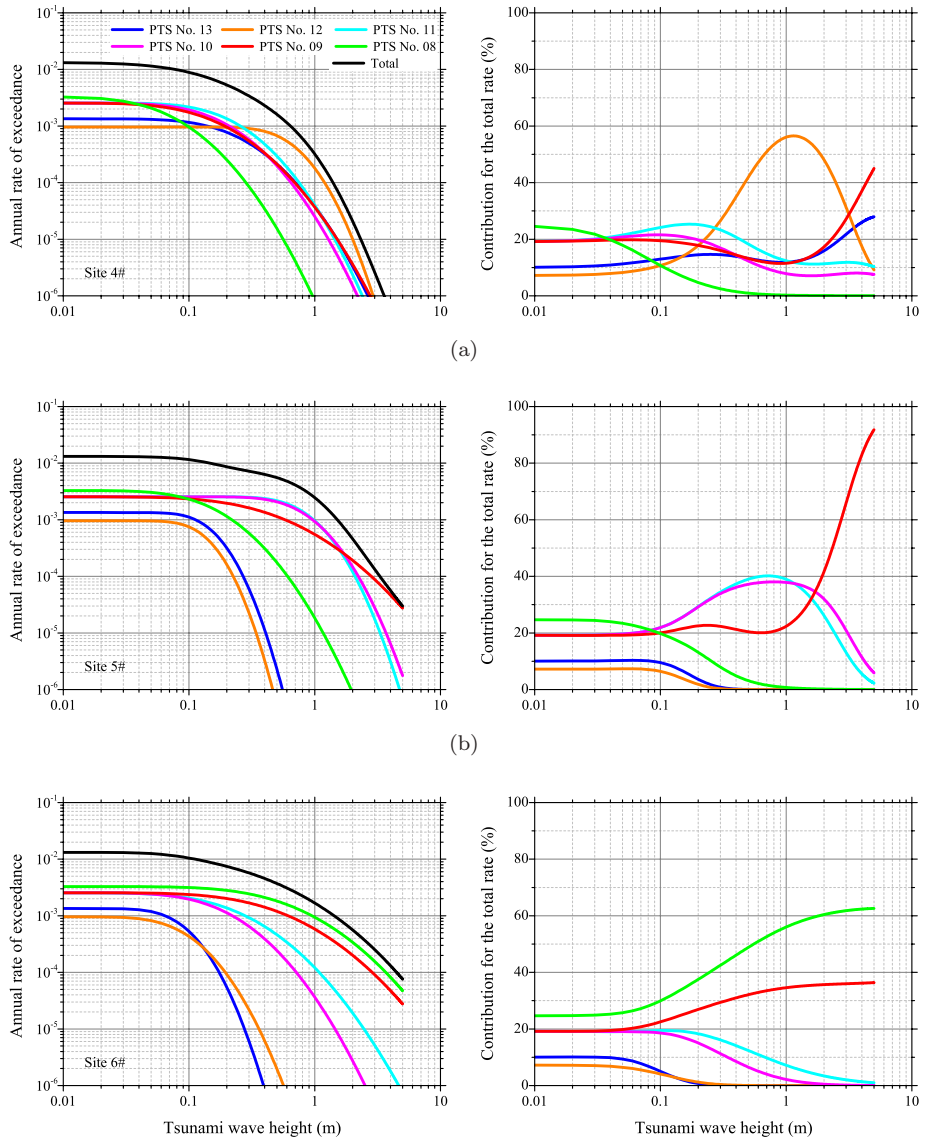

Fig. 10. Annual rate of occurrence of tsunami waves exceeding a given height for sites 4#, 5#, and 6# (Left panels) and contribution of each PTS to the computation of the total rate (Right panels).

Figure 10 shows the annual rate of occurrence of tsunami waves exceeding a given height H at sites 4#, 5#, and 6#, including the results attributed to the individual PTSs and a synthesis of all the PTSs. The contributions of each PTS were calculated using Eq. (19) and these are also shown in Fig. 10. It can be seen

that when the wave height ranges from 0.3 to 3.0 m, the total rate of occurrence at site 4# is predominantly attributed to PTS No. 12, which is because of the short distance between the source and the measured site (see Fig. 2). However, when wave height is <0.3 m, the contribution of PTS No. 12 becomes minimal because of its low annual rate of occurrence of earthquakes (see Table 2). When the wave height is >3.0 m, the contributions of PTS Nos. 9 and 13 become larger than PTS No. 12. In fact, the wave heights at site 4# are <3.0 m whether they are generated by PTS Nos. 9, 12, or 13 (see Fig. 9). The PDFs of wave height >3.0 m were estimated by extrapolation of the data <3.0 m. A similar phenomenon to that mentioned above can also be seen at site 2#.

Figure 10 shows that the total rate of occurrence at site 5# and site 6# is predominantly attributed to PTS Nos. 9–11 and PTS Nos. 8 and 9, respectively. For waves <0.2 m, the annual rate at site 4# is close to the rate at sites 5# and 6#, while it is much smaller for waves >0.5 m, and even smaller by one order of magnitude for waves >1.0 m. The curves of annual rate at sites 5# and 6# are almost the same. A possible reason for this is that the upper-limit earthquake magnitude at PTS No. 12 is 7.5, which is the major contributor for site 4#, whereas it is 8.0 for PTS Nos. 9–11 (site 5#) and 8.0 for PTS No. 8 (site 6#).

6.3. *Discussion*

For each site, we calculated both the return period of the occurrence of tsunami waves exceeding a given height using Eq. (10) and the probability of exceeding a given tsunami wave height within 100 years using Eq. (11) the results are presented in Fig. 11. For a wave height <0.1 m, the probabilities for sites 1#, 2#, and 3# are all 35%, smaller than the value of about 75% for sites 4#, 5#, and 6#. This is because only three PTSs were considered in the hazard analysis for sites 1#, 2#, and 3# (see Fig. 8), whereas six PTSs were considered in the analysis for sites 4#, 5#, and 6# (see Fig. 10).

The probabilities of sites 5# and 6# are higher than the other sites, especially for waves >1.0 m, i.e. higher than sites 1# and 4# by one order of magnitude and higher than sites 2# and 3# by two orders of magnitude. The upper-limit earthquake magnitude of PTS Nos. 8–11 is 8.0 and these sources have the greatest impact on sites 4# and 5#. The upper-limit earthquake magnitude of PTS Nos. 12–15 is 7.5 and these sources have the greatest impact on sites 1# to 4#. This shows that the upper-limit earthquake magnitude of the PTS plays an important role when assessing the tsunami hazard.

Figure 11 shows that the probability of site 3# is almost the lowest because the strike of the fault at PTS No. 12 (the closest PTS to site 3#) is aligned obliquely to the coastline, whereas the faults of the other PTSs are aligned almost parallel to the coastline. This shows that the relative geographical position of the source and the site is an important factor in assessing the tsunami hazard.

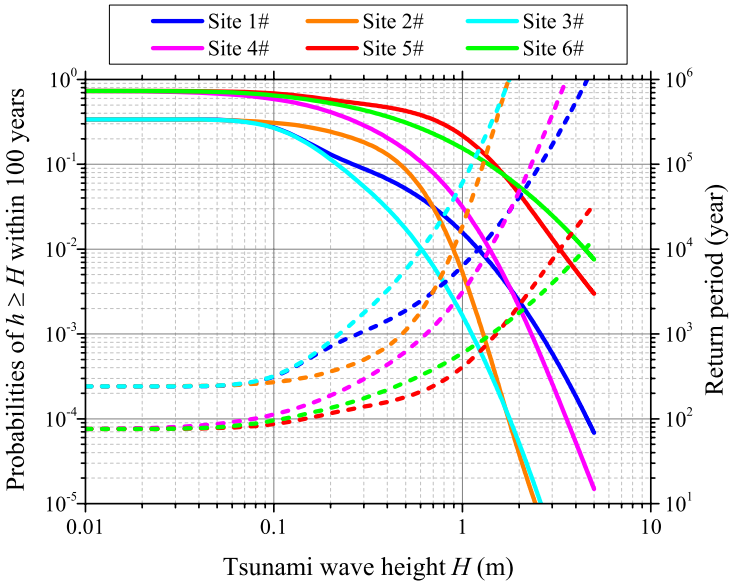

Fig. 11. Probabilities of at least one occurrence of exceedance of tsunami wave height within 100 years for sites 1# to 6# (solid lines). Dashed lines show the return period for sites from 1# to 6# where tsunami waves reach any level of tsunami wave height.

Table 3. Probabilities of at least one occurrence within 100 years and return periods of tsunami waves >0.5 and >1.0 m at the reference cities and bay of the SCS.

Measured site	Reference site	$P(h \geq H, t = 100$ years) (%)		$R(h \geq H)$ (year)	
		$H = 0.5$ m	$H = 1.0$ m	$H = 0.5$ m	$H = 1.0$ m
1#	Macao	5.17	1.57	1884	6304
2#	HongKong	8.66	0.53	1103	18,682
3#	Daya Bay	1.74	0.17	5712	60,463
4#	Shantou	14.85	3.16	622	3119
5#	Xiamen	42.60	21.81	180	407
6#	Quanzhou	31.06	15.47	269	595

Table 3 displays the return periods of the occurrence of tsunami waves >0.5 and >1.0 m, and the probabilities of at least one occurrence within 100 years for each site. The reference cities and bay that are closest to sites 1# to 6# are also presented. The probabilities of tsunami waves >0.5 and >1.0 m occurring at Xiamen and Quanzhou are 42.60% and 31.06%, and 21.81% and 15.47%, respectively. This means the tsunami hazard for these two cities is high. As mentioned above, the locations of the six measured sites have bathymetric depths of 10 m (see Fig. 2). If the sites were located within the bay or nearer land, the tsunami hazard would be much more serious because of the effects of wave convergence or run up.

Compared with Xiamen and Quanzhou in the Taiwan Strait, the tsunami hazard at Macao and Hong Kong in the Pearl River Estuary is much lower. The return

period of tsunami waves >0.5 m is >1000 years for Macao and Hong Kong, and even > 5000 years for Daya Bay. It should be noted that only local PTSs were considered in this study. If the impact of the Manila Trench were also considered, the return periods calculated in this study for sites 1# to 4# would be shortened significantly and the probabilities would be greatly increased. Liu *et al.* [2007] performed a PTHA for the Chinese coastal area using only the Manila Trench as the regional PTS. The results showed that the probability of at least one occurrence of tsunami waves >1.0 m within 100 years was 43.99% for Shantou, 27.31% for both Hong Kong and Macao, and 0.00% for Xiamen. This means both the Manila Trench and the local PTSs are of relevance to the Chinese coastal area south of Taiwan, but only the local PTSs are of relevance to the area within the Taiwan Strait.

7. Conclusions

To apply a PTHA to the Southern coast of China we delineated some local PTSs, determined some parameters of seismic activity for each source, and selected six typical measured sites for case studies to demonstrate the proposed Chinese PTHA. Based on the results, the following conclusions were drawn:

(1) Using the data from the latest issued national "Seismic ground motion parameters zonation map of China (GB 18306-2015)", eight PTSs, Nos. 8–15, were delineated and the parameters of their seismic activity were determined, including the upper-limit earthquake magnitude M_u, the value of constant b of the Gutenberg−Richter recurrence law, and the annual rate of earthquake occurrence v.
(2) The tsunami scenarios triggered by earthquake magnitudes of 7.0 and 7.5 for PTS Nos. 13–15 show that the areas affected by the tsunami waves generated by the local PTSs are not very large. For the PTHA, PTS Nos. 13–15 were considered for the Pearl River Estuary and PTS Nos. 8–13 were considered for the Taiwan Strait. The lower-limit earthquake magnitude was set at 7.0.
(3) Six measured sites were selected in the Pearl River Estuary and the Taiwan Strait for use as PTHA case studies. They were referenced to Macao, Hong Kong, Shantou, Xiamen, Quanzhou, and Daya Bay, which are located close to these sites. For each site, the annual rate of occurrence of tsunami waves exceeding a given height was calculated, including that attributed to the individual PTSs and to a synthesis of all the PTSs. The comparison between the different sites and between different PTSs showed that the upper-limit earthquake magnitude of the PTSs and the relative spatial geographical position between the measured site of interest and the PTS were two important factors that affect the PTHA.
(4) Finally, the probabilities of at least one occurrence within 100 years and the return periods of tsunami waves exceeding a given height were calculated for each site. The results showed that the probabilities were 5–10% in Macao and

Hong Kong, but 30–40% in Xiamen and Quanzhou for tsunami waves >0.5 m. The return periods were only 400–600 years in Xiamen and Quanzhou for tsunami waves >1.0 m. If the Manila Trench were also considered as a regional source, the return periods would be shortened and the probabilities increased. It is concluded that the tsunami hazard for the southern coast of China is very high, and that both local and regional PTSs should be included in any future PTHA.

Since the worst case was considered in this study that all PTSs were assumed as thrust type, we believe the estimated tsunami hazard for the southern coast of China may be probably higher than the real situation. As a result, caution should be exercised when the PTHA results of this study are used for further studies or engineering practice, especially for policy-making of disaster mitigation. If in-depth investigation on the source mechanism and parameters of each PTS could be done, and the uncertainty analysis also could be included, the PTHA results will become more accurate and valuable.

Acknowledgments

We thank two anonymous reviewers for their valuable suggestions and constructive comments, which have improved considerably the quality of the manuscript. This work is supported by the Scientific Research Fund of Institute of Engineering Mechanics, China Earthquake Administration No. 2014B06, National Natural Science Fund No. 51278473, and the Environmental Protection Research Fund for Public Interest No. 201209040. We would like to thank Dr. Xiaoming Wang for providing help with the COMCOT model.

References

Aki, K. [1966] "Generation and propagation of G waves from the Niigata earthquake of June 14, 1964. Part 2, Estimation of earthquake moment, released energy and stress-strain drop from G wave spectrum," *Bull. Earthq. Res. Inst.* **44**, 73–88.

Annaka, T., Satake, T., Sakakiyama, T., Yanagisawa, K. and Shuto, N. [2007] "Logic-tree approach for probabilistic tsunami hazard analysis and its applications to the Japanese coasts," *Pure Appl. Geophys.* **164**, 577–592.

Burbidge, D., Cummins, P. R., Mleczko, R. and Thio, H. K. [2008] "Probabilistic tsunami hazard assessment for Western Australia," *Pure Appl. Geophys.* **165**, 2059–2088.

Chau, K. T. [2008] "Tsunami hazard along coasts of China: A re-examination of historical data," *The 14th World Conf. Earthquake Engineering*, Beijing, China.

Chen, G. X. and Zhou, B. G. [2011] "Determination of seismic belts and potential seismic sources in China and its surrounding area," Technique Report of the Seismic Ground Motion Parameter Zonation Map of China, China Earthquake Administration, p. 669. (in Chinese).

Choi, B. H., Min, B. I., Pelinovsky, E., Tsuji, Y. and Kim, K. O. [2012] "Comparable analysis of the distribution functions of runup heights of the 1896, 1933 and 2011 Japanese Tsunamis in the Sanriku area," *Nat. Hazards Earth Syst. Sci.* **12**(5), 1463–1467.

Choi, B. H., Pelinovsky, E., Ryabov, I. and Hong, S. J. [2002] "Distribution functions of tsunami wave heights," *Nat. Hazards* **25**(1), 1–21.

Cornell, C. A. [1968] "Engineering seismic risk analysis," *Bull. Seismol. Soc. Am.* **58**(5), 1583–1606.

Dao, M. H., Pavel, T., Chan, E. S. and Kusnowid, M. [2009] "Tsunami propagation scenarios in the South China Sea," *J. Asia Earth Sci.* **36**(1), 67–73.

Gao, M. T. [2015] *Manual for National Code "Seismic Ground Motion Parameters Zonation Map of China (GB 18306-2015)"* (Standards Press of China, Beijing).

Geist, E. L. and Parsons, T. [2006] "Probabilistic analysis of tsunami hazards," *Nat. Hazards* **37**(3), 277–314.

Gonzalez, F. I., Geist, E. L., Jaffe, B., Kanoglu, U., Mofjeld, H., Synolakis, C. E., Titov, V. V., Arcas, D., Bellomo, D., Carlton, D., Horning, T., Johnson, J., Newman, J., Parsons, T., Peters, R., Peterson, C., Priest, G., Venturato, A., Weber, J., Wong, F. and Yalciner, A. [2009] "Probabilistic tsunami hazard assessment at Seaside, Oregon, for near- and far-field seismic sources," *J. Geophys. Res. Oceans* **114**(C11), C11023.

Grezio, A., Marzocchi, W., Sandri, L. and Gasparini, P. [2010] "A Bayesian procedure for probabilistic tsunami hazard assessment," *Nat. Hazards* **53**, 159–174.

Hanks, T. C. and Kanamori, H. [1979] "A moment magnitude scale," *J. Geophys. Res.* **84**(B5), 2348–2350.

Hou, J. M., Li, X. J., Yuan, Y. and Wang, P. T. [2016] "Tsunami hazard assessment along the Chinese mainland coast from earthquakes in the Taiwan region," *Nat. Hazards* **82**(2), 1269–1281.

Houston, R., Carver, R. D. and Markle, D. G. [1977] "Tsunami-wave elevation frequency of occurrence for the Hawaiian Islands," U.S. Army Corps of Engineers Waterways Experiment Station Technical Report, H-77-16.

Huang, Z. H., Wu, T. R., Tan, S. K., Megawati, K., Shaw, F., Liu, X. Z. and Pan, T. C. [2009] "Tsunami hazard from the subduction Megathrust of the South China Sea: Part II. Hydrodynamic modeling and possible impact on Singapore," *J. Asia Earth Sci.* **36**(1), 93–97.

Kelvin, B. [2005] "Review of tsunami hazard and risk in New Zealand," Institute of Geological & Nuclear Sciences Client Report, 2005/104.

Kulikov, E. A., Rabinovich, A. B. and Thomson, R. E. [2005] "Estimation of tsunami risk for the coasts of Peru and northern Chile," *Nat. Hazards* **35**(2), 185–209.

Lau, A. Y. A., Switzer, A. D., Dominey-Howes, D., Aitchison1, J. C. and Zong, Y. [2010] "Written records of historical tsunamis in the northeastern South China Sea — challenges associated with developing a new integrated database," *Nat. Hazards Earth Syst. Sci.* **10**(9), 1793–1806.

Liu, Y., Santos, A., Wang, S. M., Shi, Y. L., Liu, H. L. and Yuen, D. A. [2007] "Tsunami hazards along Chinese coast from potential earthquakes in South China Sea," *Phys. Earth Planet. Inter.* **163**(4), 233–244.

Liu, P. L. F., Wang, X. M. and Salisbury, A. J. [2009] "Tsunami hazard and early warning system in South China Sea," *J. Asia Earth Sci.* **36**(1), 2–12.

Mak, S. and Chan, L. S. [2007] "Historical tsunamis in South China," *Nat. Hazards* **43**, 147–164.

Megawati, K., Shaw, F., Si, K., Huang, Z. H., Wu, T. R., Lin, Y., Tan, S. K. and Pan, T. C.[2009] "Tsunami hazard from the subduction megathrust of the South China Sea: Part I. Source characterization and the resulting tsunami," *J. Asia Earth Sci.* **36**(1), 13–21.

Okal, E. A., Synolakis, C. E. and Kalligeris, N. [2011] "Tsunami simulations for regional sources in the South China and adjoining seas," *Pure Appl. Geophys.* **168**(6), 1153–1173.

Pan, W. L., Wang, S. A. and Cai, S. Q. [2009] "Simulation of potential tsunami hazards in the South China Sea," *Pure Appl. Geophys.* **28**(6), 7–14 (in Chinese).

Papadopoulos, G. A., Daskalaki, E., Fokaefs, A. and Giraleas, N. [2010] "Tsunami hazard in the eastern Mediterranean sea strong earthquakes and tsunamis in the West Hellenic arc and trench system," *J. Earthq. Tsunami* **4**(3), 145–179.

Papazachos, B. C., Scordilis, E. M., Panagiotopoulos, D. G., Papazachos, C. B. and Karakaisis, G. F. [2004] "Global relations between seismic fault parameters and moment magnitude of earthquakes," *Bull. Geol. Soc. Greece* **36**, 1482–1489.

Pei, S. P., Xu, Z. H. and Wang, S. Y. [2004] "Sn wave tomography in the uppermost mantle beneath the China continent and adjacent regions," *Chinese J. Geophys.* **47**(2), 250–256 (in Chinese).

Ren, Y. F., Wen, R. Z., Zhou, B. F. and Shi, D. C. [2010] "Deterministic analysis of the tsunami hazard in China," *Sci. Tsunami Hazards* **29**(1), 32–42.

Ren, Y. F., Wen, R. Z. and Song, Y. Y. [2014] "Recent progress of tsunami hazard mitigation in China," *Episodes* **37**(4), 277–283.

Rikitake, T. and Aida, I. [1988] "Tsunami hazard probability in Japan," *Bull. Seismol. Soc. Am.* **78**(3), 1268–1278.

Suppasri, A., Imamura, F. and Koshimura, S. [2012] "Tsunami hazard in the eastern Mediterranean sea strong earthquakes and tsunamis in the West Hellenic arc and trench system," *J. Earthq. Tsunami* **6**(2), 1250011-1–27.

Thio, H. K., Somerville, P. and Ichinose, G. [2007] "A probabilistic analysis of strong ground motion and tsunami hazards in Southeast Asia", *J. Earthq. Tsunami* **1**(2), 119–137.

Thio, H. K., Somerville, P. and Polet J. [2010] "Probabilistic tsunami hazard in California," Pacific Earthquake Engineering Research Center Report, 2010/108, p. 331.

Tinti, S. [1991] "Assessment of tsunami hazard in the Italian seas," *Nat. Hazards* **4**(2–3), 267–283.

Wells, D. L. and Coppersmith, K. J. [1994] "New empirical relationships among magnitude, rupture length, rupture width, rupture area, and surface displacement," *Bull. Seismol. Soc. Am.* **84**(4), 974–1002.

Wen, R. Z. and Ren, Y. F. [2007] "Preliminary study on tsunami hazard analysis in China," *World Earthq. Eng.* **23**(1), 6–11 (in Chinese).

Wen, R. Z., Ren, Y. F., Li, X. J. and Pan, R. [2011] "Probability analysis method of earthquake-induced tsunami risk in China," *South China J. Seismol.* **31**(4), 1–13 (in Chinese).

Wu, T. R. [2012] "Deterministic study on the potential large tsunami hazard in Taiwan," *J. Earthq. Tsunami* **6**(3), 1250034–1–18.

Wu, T. R. and Huang, H. C. [2009] "Modeling tsunami hazards from Manila trench to Taiwan," *J. Asia Earth Sci.* **36**(1), 21–28.

Yang, M. L. and Wei, B. L. [2005] "The potential seismic tsunami risk in South China Sea and it's surrounding region," *J. Catastrophol.* **20**(3), 41–47 (in Chinese).

Zhang, H. N. [1995] "Seismic activity and regional stability for the South China Sea and its surrounding area," *Acta Oceanol. Sin.* **17**(6), 81–89 (in Chinese).

Zhang, X. R. and Chen, G. T. [1983] "On the focal mechanisms of earthquakes and regional stress field of the Fujian-Taiwan region," *Acta Seismol. Sin.* **5**(4), 397–411 (in Chinese).

Zhang, S. N., Jiang, J. H. and Chen, Y. L. [2011] "Documentation and compilation of historical earthquakes in Taiwan," Technical Report on the topic of earthquakes of CWB, Taiwan, Vol. 60, 427–448.